Magnetic properties, magnetic structure, and possible magnetoelectric effect in orthorhombic corundumlike Li₂Ni₂W₂O₉

Simon Redor [1,2] Maxim Avdeev [3,4] David Hrabovsky,[2,5] Jean-Marie Tarascon,[1] and Gwenaëlle Rousse [1,2,*]

[1]*Chimie du Solide et de l'Energie, UMR 8260, Collège de France, 75231 Cedex 05 Paris, France*
[2]*Sorbonne Université, 4 Place Jussieu, F-75005 Paris, France*
[3]*Australian Nuclear Science and Technology Organisation, Lucas Heights, New South Wales 2234, Australia*
[4]*School of Chemistry, The University of Sydney, Sydney, New South Wales 2006, Australia*
[5]*Plateforme Mesures Physiques à Basses Températures (MPBT), Sorbonne Université, 75005 Paris, France*

The magnetoelectric effect is an appealing property displayed by most compounds in the corundum-derived 429 series ($M_4A_2O_9$, A = Nb or Ta). The exception is Ni₄Nb₂O₉, crystallizing in the orthorhombic *Pbcn* space group: because of symmetry considerations, its magnetic space group forbids the occurrence of the magnetoelectric effect. Li₂Ni₂W₂O₉ crystallizes in the same space group as Ni₄Nb₂O₉; however, as half the Ni^{2+} cations are replaced by Li$^+$ cations, the interactions between the remaining magnetic elements are drastically modified. In this paper, we present the results of magnetic bulk measurements, showing an antiferromagnetic ordering coupled with strong ferromagnetic interactions below $T_N \approx 8$ K in Li₂Ni₂W₂O₉. Through neutron diffraction, the magnetic structure of Li₂Ni₂W₂O₉ is solved, and it is confidently established that it presents the $Pb'c'n'$ Shubnikov space group (#60.425), whose point symmetry $m'm'm'$ allows the magnetoelectric effect. This could possibly open the door to a family of magnetoelectric, orthorhombic compounds.

I. INTRODUCTION

The 429 family is a series of compounds with general formula $M_4A_2O_9$ (M = Mg, Mn, Fe, Co, Ni; A = Nb, Ta). Described by Bertaut *et al.* [1], these materials sparked interest in recent years because of their magnetic properties, especially their magnetoelectric properties [2–6]. The linear magnetoelectric effect is a coupling between the electric and magnetic responses of a material: an electric polarization of the material can be induced by a magnetic field, and its magnetization can be induced by an electric field. It has been demonstrated that the existence of this effect in a material relies on its magnetic structure, particularly its magnetic point symmetry [7–11]. Most 429 compounds crystallize in the trigonal space group $P\bar{3}c1$, in a structure derived from that of corundum (α-Al₂O₃) [1,12]. This often leads to magnetic structures with point symmetries compatible with the magnetoelectric effect, such as $2/m'$ in Co₄Nb₂O₉ [13–16], $2/m'$ and $2'/m$ in Fe₄Nb₂O₉ [17], or $\bar{3}'m'$ in Mn₄Nb₂O₉ [1], to give a few examples.

Ni₄Nb₂O₉ is an outlier in the 429 family. Although its crystal structure is very similar to corundum, slight differences in the Ni positions make it crystallize in the orthorhombic *Pbcn* space group [18], instead of the usual trigonal $P\bar{3}c1$ seen in other 429 compounds. Ni₄Nb₂O₉ displays interesting magnetic properties originating from the $3d^8$ electronic configuration of Ni^{2+}; specifically, it has been studied for its ferrimagnetism [19,20] and magnetization reversal effects [21–23]. However, the magnetic space group of this material is $Pb'cn'$ with magnetic point group $m'm'm$ (#8.4.27), and thus, it does not allow a magnetoelectric coupling [24].

A few studies have been conducted on exotic magnetic materials based on Ni₄Nb₂O₉. These materials are usually prepared through the partial substitution of the Ni^{2+} cations by another divalent cation. Tarakina *et al.* [25] reported on compounds with the general formula Mg$_{4-x}$Ni$_x$Nb₂O₉ ($0 \leqslant x \leqslant 4$), showing that, for $x > 2.75$, the *Pbcn* structure and the magnetic properties of Ni₄Nb₂O₉ were maintained, although planar defects were introduced in the structure. Later, Bolletta *et al.* [21] worked on tuning the magnetization reversal effect in Ni₄Nb₂O₉ through partial substitution of nickel with zinc, showing significant changes of magnetic properties in Ni$_{4-x}$Zn$_x$Nb₂O₉ compounds, from $x = 0$ to 0.75. More recently, Jiongo-Dongmo *et al.* [22] studied the Co₄Nb₂O₉ − Ni₄Nb₂O₉ phase diagram (Ni$_{4-x}$Co$_x$Nb₂O₉), aiming to combine the linear magnetoelectric effect of the former with the magnetization reversal of the latter. They showed a nice transition from the *Pbcn* structure to the $P\bar{3}c1$ structure for x between 2.2 and 2.5. However, the linear magnetoelectric effect could not be observed in the *Pbcn* structure for this series of compounds.

The crystal structure of Li₂Ni₂W₂O₉ was recently reported [26]. Like Ni₄Nb₂O₉, Li₂Ni₂W₂O₉ crystallizes in a corundumlike *Pbcn* structure. However, the Nb₂O₉ dimers found in Ni₄Nb₂O₉ are replaced by W₂O₉ dimers, allowing half the Ni^{2+} cations to be substituted by Li$^+$ cations to ensure charge neutrality. Specifically, the Li$^+$ cations are arranged in a honeycomb configuration in between the (Ni, W) layers (Fig. 1). This structural peculiarity might change radically the magnetic interactions between Ni^{2+} cations in Li₂Ni₂W₂O₉ compared with Ni₄Nb₂O₉.

*gwenaelle.rousse@upmc.fr

054105-1
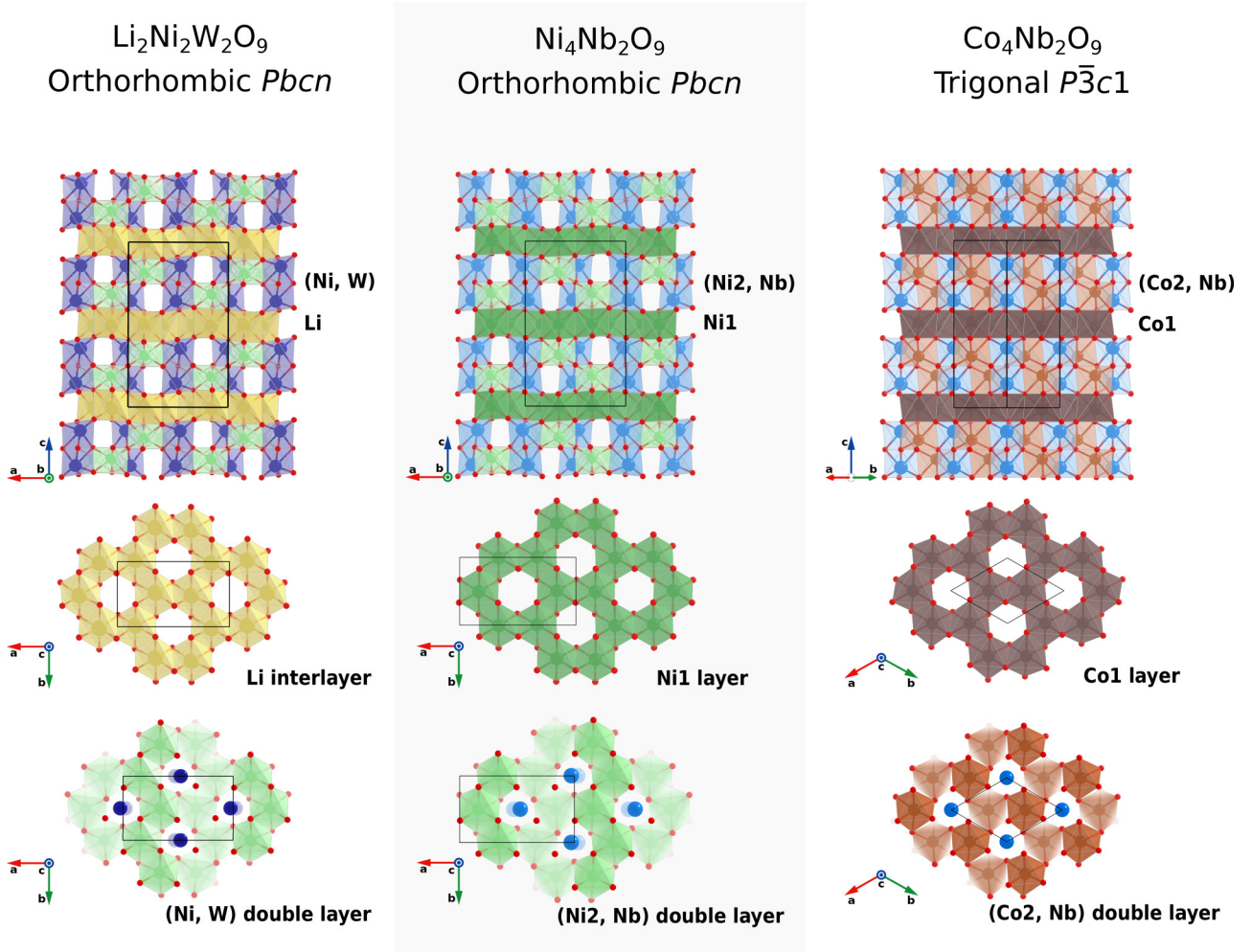
FIG. 1. Crystal structures of $Li_2Ni_2W_2O_9$ (left), $Ni_4Nb_2O_9$ (middle), and $Co_4Nb_2O_9$ (right). Oxygen atoms are red, tungsten atoms are dark blue, and niobium atoms are sky blue; lithium atoms are yellow, nickel atoms in various shades of green, and cobalt atoms in various shades of brown. For the double layer view, atoms in a paler color are at lower z coordinates.

Herein, we present a preliminary study of the magnetic properties of $Li_2Ni_2W_2O_9$. An antiferromagnetic ordering is observed below $T_N \approx 8$ K, while modified Curie-Weiss fits suggest strong ferromagnetic interactions. Neutron powder diffraction allowed us to confidently solve the magnetic structure of the material; the magnetic properties are well explained by a magnetic lattice in the $Pb'c'n'$ Shubnikov space group (#60.425) with magnetic point group $m'm'm'$ (#8.5.28), which is neither polar nor ferromagnetic but allows magnetoelectric coupling in the material [8–11].

A. Experimental methods

1. Reagents

$Li_2Ni_2W_2O_9$ powder was synthesized from lithium carbonate powder (Li_2CO_3, Sigma-Aldrich, $\geqslant 99.0\%$), nickel oxide powder (NiO, Sigma-Aldrich, 99%), and tungsten trioxide powder (WO_3, Alfa Aesar, 99.8%).

2. Synthesis

$Li_2Ni_2W_2O_9$ powder was obtained by solid-state synthesis. The full process was detailed elsewhere [26]. In summary,

Li_2CO_3, NiO, and WO_3 powders were mixed in stoichiometric amounts, first with an agate mortar, then for 30 min in a steel jar with one steel ball using a mechanical SPEX SamplePrep 8000M Mixer/Mill. The resulting mix was then heated in an alumina crucible in air, using a Carbolite CWF 1200 muffle furnace. The mix was first heated at 650 °C for 12 h (heating rate: +5 °C/min), then to 700 °C for 24 h (heating rate: +2 °C/min). Then the annealed powder was ball milled for 30 min and annealed again at 700 °C for 24 h in air (heating rate: +5 °C/min). This milling-annealing step was repeated one more time to remove most of the impurities in the powder.

The purity of the final product was evaluated through powder x-ray diffraction (XRD) measurements (Fig. 2), using a Bruker D8 Advance lab diffractometer equipped with a Cu $K\alpha$ source ($\lambda_1 = 1.54056$ Å and $\lambda_2 = 1.54439$ Å), and a LynxEye-2 detector. The measurements were performed in the Bragg-Brentano configuration.

3. Magnetic properties

The magnetic properties of $Li_2Ni_2W_2O_9$ were assessed using a Quantum Design MPMS3 superconducting quan-

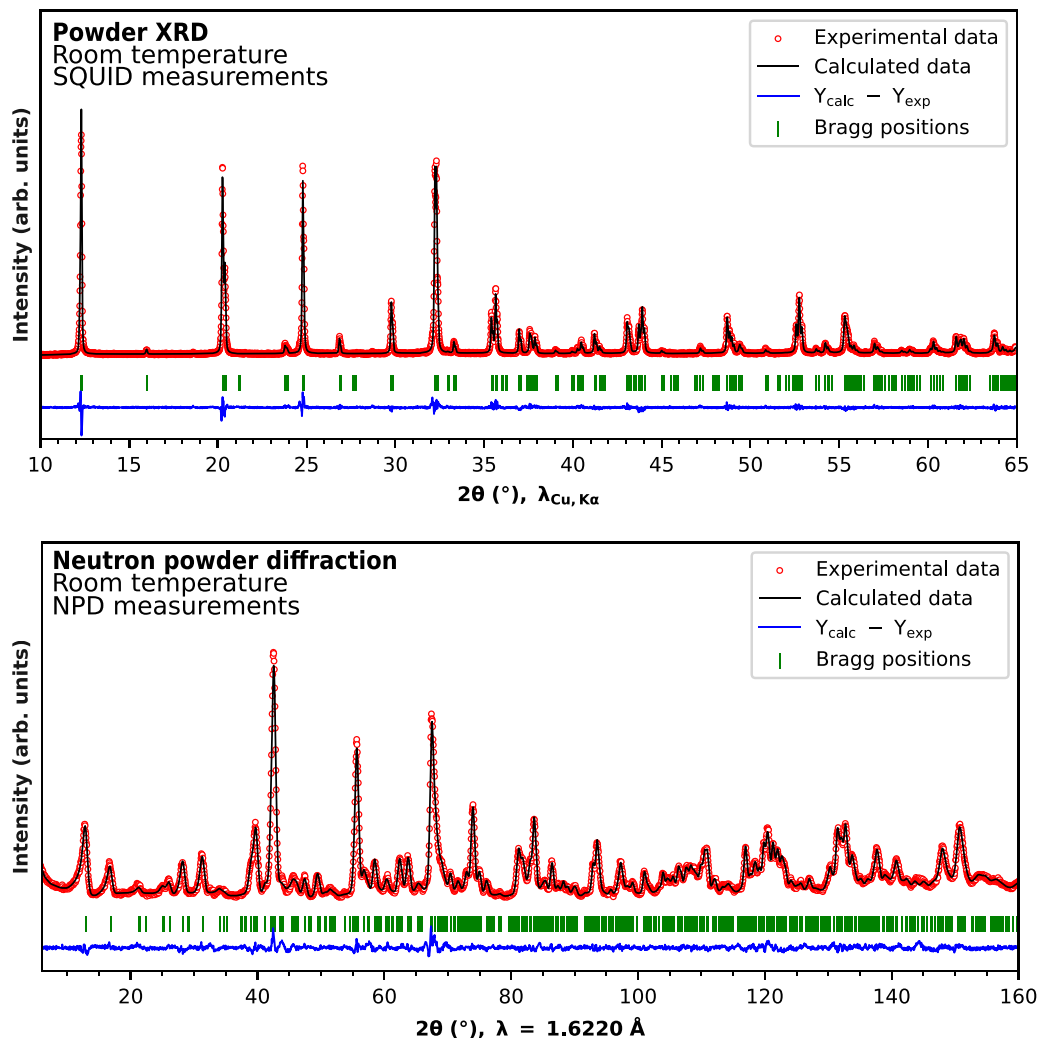FIG. 2. Top: Rietveld refinement of the powder x-ray diffraction (XRD) pattern for a typical $Li_2Ni_2W_2O_9$ sample used for the magnetic bulk measurements. Bottom: Rietveld refinement of the neutron powder diffraction pattern at room temperature for the $Li_2Ni_2W_2O_9$ sample used for all neutron diffraction measurements.

tum interference device (SQUID). A few milligrams of $Li_2Ni_2W_2O_9$ powder were compressed in a plastic capsule and placed in a brass sample holder for the measurements.

Longitudinal magnetic moment (M) measurements were performed in a DC magnetic field ($H = 200$ Oe, 1 kOe, or 10 kOe), with temperatures ranging from 1.8 to 300 K; the measurements were performed in field-cooled (FC) and zero-field-cooled (ZFC) modes. Magnetization curves were obtained for $T = 2$ and 100 K, with H ranging from -70 to 70 kOe.

4. Neutron diffraction

Neutron powder diffraction measurements were performed using the Echidna diffractometer [27] ($\lambda_{LT} = 2.4395$ Å or $\lambda_{RT} = 1.6220$ Å) at the Open Pool Australian Lightwater (OPAL) reactor of the Australian Nuclear Science and Technology Organisation (ANSTO). The measurements were performed at room temperature ($\lambda = \lambda_{RT}$), then at $T = 15$, 7, 5, and 3.5 K ($\lambda = \lambda_{LT}$), using roughly 2 g of $Li_2Ni_2W_2O_9$ powder placed in a vanadium can.

The powder diffraction patterns were analysed according to the Rietveld method [28] with the FULLPROF suite [29]. The

magnetic form factor of Ni^{2+} was used to solve and refine the magnetic structure.

II. RESULTS

A. Structural characterization

In this paper, different $Li_2Ni_2W_2O_9$ samples were used for magnetic bulk measurements and for low-temperature neutron powder diffraction measurements. The Rietveld refinements for their room-temperature XRD and neutron powder diffraction data, respectively, are shown in Fig. 2.

For both samples, the experimental patterns can be nicely fitted with the crystal structure reported for $Li_2Ni_2W_2O_9$, in the *Pbcn* space group and with lattice parameters $a \approx 8.70$ Å, $b \approx 5.06$ Å, and $c \approx 14.35$ Å (Tables I and S1 and S2 in the Supplemental Material [30]). Both samples are of high purity and were deemed of good enough quality for the subsequent measurements.

B. Magnetic properties

Molar magnetic susceptibility (χ_m) measurements performed on $Li_2Ni_2W_2O_9$ powder, in ZFC and FC modes, are

TABLE I. Lattice parameters deduced from the Rietveld refinements of the room temperature powder XRD and neutron powder diffraction data for $Li_2Ni_2W_2O_9$ samples.

Sample	a (Å)	b (Å)	c (Å)	R_{Bragg} (%)
LNWO SQUID	8.69663(7)	5.06468(4)	14.3514(11)	6.60
LNWO neutron	8.69523(8)	5.06407(5)	14.3451(18)	3.32

shown in Fig. 3. For an applied magnetic field H of 200 Oe or 1 kOe, the material displays a paramagnetic behavior down to a temperature T_N of roughly 8 to 9 K. At this Néel point, a cusp can be observed, characteristic of an antiferromagnetic transition. However, such a transition is no longer apparent when the applied field is increased to 10 kOe, suggesting that the magnetic properties of the material are field dependent. Magnetization measurements were performed to confirm this observation and are displayed in Fig. 4.

At 100 K, the magnetization curve is linear, indicating a fully paramagnetic behavior, which does not seem impacted by the applied magnetic field. In contrast, at 2 K, below T_N, inflexion points can be observed in the magnetization curve for $|H| \approx 8$ kOe, indicating a change in magnetic behavior. This behavior could be associated to a metamagnetic transition [31], but this needs to be confirmed through neutron diffraction measurements in an applied magnetic field, which were not conducted in this paper.

The curves for $1/\chi_m$ vs T were fitted with a modified Curie-Weiss law [Eq. (1)]:

$$\chi_m = \chi_0 + \frac{C}{T - \theta_{CW}}, \tag{1}$$

where χ_0 is a temperature-independent contribution to the magnetic susceptibility in mol^{-1}, C is the Curie constant in $m^3 K mol^{-1}$ and θ_{CW} is the Curie-Weiss temperature in K. Results of the fits are shown in Table II. The fitting range had to be adapted from one measurement to the next to account for deviations from the model due to magnetic impurities. Interestingly, even though the shape of the susceptibility curves clearly proves that $Li_2Ni_2W_2O_9$ goes through an antiferromagnetic ordering at low temperatures (for $H < 8$ kOe), the values of θ_{CW} are all positive, which indicates that there are strong ferromagnetic interactions in the material.

One can calculate the effective moment per magnetic ion μ_{eff} from the values of C, using Eq. (2) [32]:

$$\mu_{eff} = \sqrt{\frac{3k_B}{N_A\mu_0\mu_B^2}}\sqrt{C} \tag{2}$$

where k_B is the Boltzmann constant (1.38×10^{-23} J K^{-1}), N_A is the Avogadro constant (6.022×10^{23} mol^{-1}), μ_0 is the magnetic constant ($4\pi \times 10^{-7}$ H m^{-1}), and μ_B is the Bohr magneton (9.274×10^{-24} J T^{-1}). Aside from the aberrant 3.8 μ_B value calculated for the FC curve at $H = 200$ Oe (which is probably related to impurities in the sample), the calculated values of μ_{eff} for the Ni^{2+} cations in $Li_2Ni_2W_2O_9$ range from 3.3 to 3.4 μ_B. These experimental values land between the theoretical values for Ni^{2+} in an octahedral coordination, with and without orbital angular momentum (4.47 and 2.83 μ_B, respectively); thus, there must be some weak contribution from the orbital angular momentum to the magnetic moment. This

matches quite well with empirical values previously reported in the literature [24,33].

The frustration index for $Li_2Ni_2W_2O_9$ f can also be calculated from θ_{CW} and T_N, using Eq. (3):

$$f = \left|\frac{\theta_{CW}}{T_N}\right|. \tag{3}$$

Estimating that T_N is roughly equal to 8 K leads to values of f ranging from 1.1 to 1.9: the magnetic structure is not heavily frustrated.

C. Magnetic structure

To solve the magnetic structure of $Li_2Ni_2W_2O_9$ and obtain a better understanding of the results obtained from the bulk magnetic measurements, low-temperature powder neutron diffraction experiments were conducted. Neutron diffraction scans were performed between 15 and 3.5 K, above and below the Néel point (Fig. 5).

Starting at 7 K, a peak appears at $2\theta = 16.06°$; this peak is not present in the diffractogram for $T = 15$ K, and it keeps increasing as the temperature gets lower. This confirms that there is indeed a magnetic ordering for $T < 8$ K. Similarly, another peak seems to increase in intensity as the temperature is decreased, at $2\theta = 9.55°$. Aside from these changes, there is no significant shift in positions or intensities for the nuclear Bragg peaks upon the sample cooling down, indicating that the nuclear crystal structure remains the same below the magnetic transition temperature.

The nuclear structure of $Li_2Ni_2W_2O_9$ was solved in a previous work [26] and was used as a basis to solve the magnetic structure. $Li_2Ni_2W_2O_9$ crystallizes in the orthorhombic *Pbcn* space group. The positions of the noticeable magnetic reflections at $2\theta = 9.55°$ and $16.06°$ in the neutron diffraction patterns match with the (001) and (100) Bragg positions for the parent space group, in the same unit cell as the nuclear structure. Therefore, the propagation vector for the magnetic structure is $\mathbf{k} = (0, 0, 0)$, as the magnetic and nuclear unit cells are identical.

Based on the Miller indexes for the magnetic peaks (001) and (100), it can be ascertained that components of the magnetic moments of the nickel cations are perpendicular to the reciprocal space basis vectors $\mathbf{c}^*$ and $\mathbf{a}^*$; for an orthorhombic space group, $\mathbf{c}^*$ and $\mathbf{a}^*$ are collinear to the c and a axes, respectively. Simulations, based on the nuclear structure of $Li_2Ni_2W_2O_9$, were performed using the FULLPROF software [29] in the eight corresponding Shubnikov magnetic space groups (*Pbcn*, *Pb'cn*, *Pbc'n*, *Pbcn'*, *Pbc'n'*, *Pb'cn'*, *Pb'c'n*, and *Pb'c'n'*), which are compatible with $\mathbf{k} = (0, 0, 0)$ and a magnetic atom in the 8d (x, y, z) site. Only two magnetic space groups lead to the appearance of the (001) and (100) diffraction peaks (Figs. S1–S8 in the Supplemental Material [30]): *Pbcn*, with two magnetic components along the a and b axes (Fig. S1 in the Supplemental Material [30]), and *Pb'c'n'*, with two magnetic components along the b and c axes (Figs. 6 and S2 in the Supplemental Material [30]). However, the best Rietveld [28] refinement was obtained when using the latter as the model for the calculations (Figs. 7 and S9 in the Supplemental Material [30]). The symmetry of *Pb'c'n'* allows all three magnetic moment components for the Ni site,
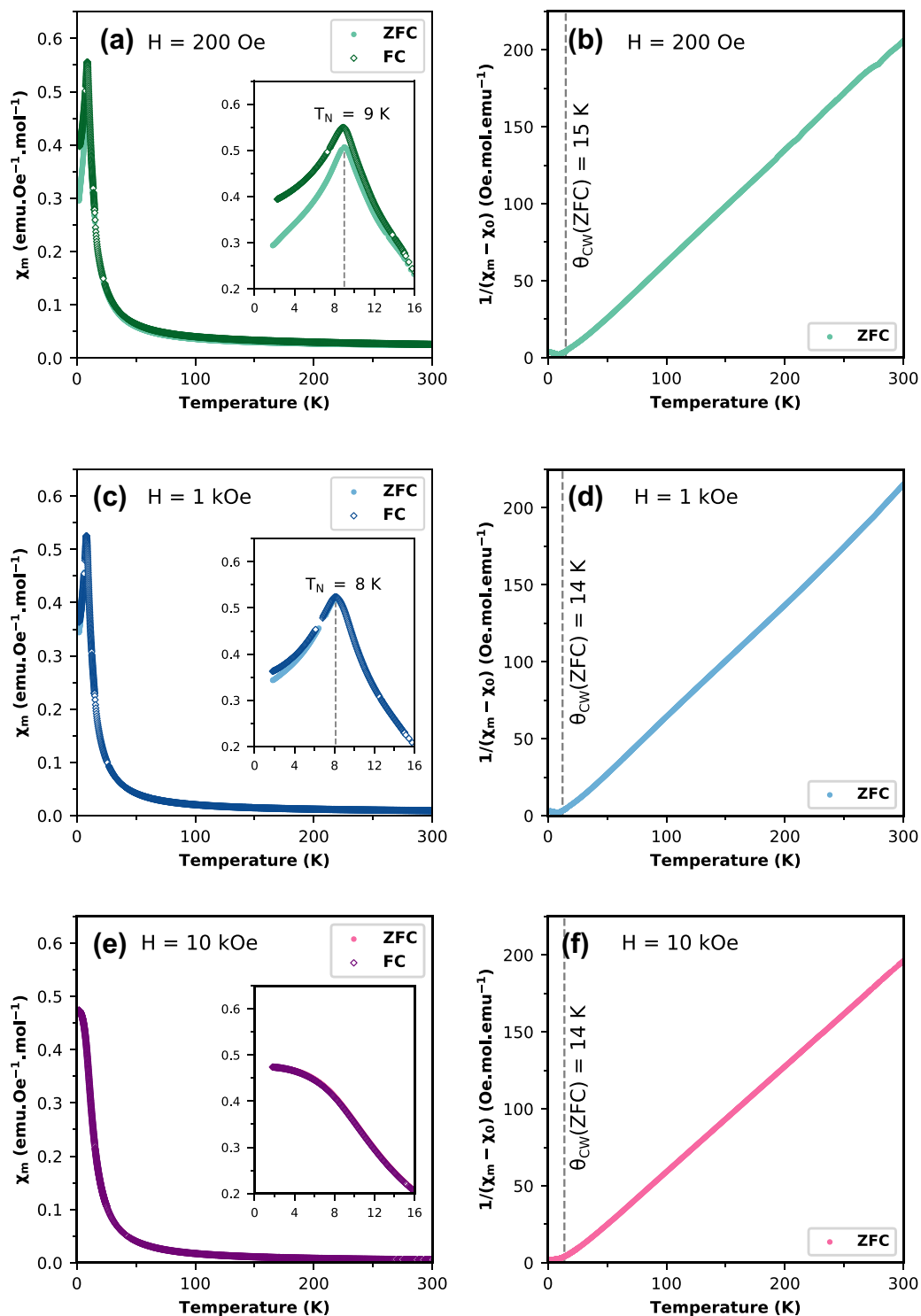
FIG. 3. Molar magnetic susceptibility (χ_m) vs T curves and $1/(\chi_m - \chi_0)$ vs T curves for (a) and (b) $H = 200$ Oe, (c) and (d) $H = 1$ kOe, and (e) and (f) $H = 10$ kOe.

but the data showed no evidence of M_x, and it was fixed to zero in the final refinement. The results of this refinement can be found in Table III and the resulting magnetic structure in Fig. 8.

All nickel cations have a small component along the b axis ($|M_y| = 0.51(6)\,\mu_\text{B}$) and a larger component along the c axis ($|M_z| = 1.49(5)\,\mu_\text{B}$), for a total magnetic moment of

1.58(5) μ_B per nickel cation. This is in reasonable agreement with the expected $2\,\mu_\text{B}$ for Ni^{2+}, with $S = 1$ in a d^8 electronic configuration. The spin-sequence along the b axis is $(+ - + - - + - +)$, and it is $(+ + - - - - + +)$ along the c axis. This leads to a canted, antiferromagnetic structure, in accordance with the antiferromagnetic transition observed in the magnetization measurements. Moreover, the
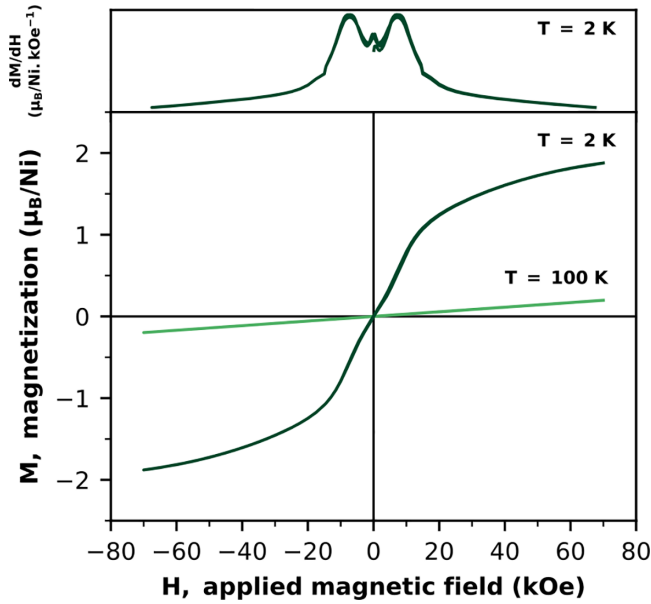
FIG. 4. Magnetization curves for $Li_2Ni_2W_2O_9$ powder at $T = 2$ K (dark green) and $T = 100$ K (light green). The derivative curve for $T = 2$ K is displayed on the upper part of the figure.
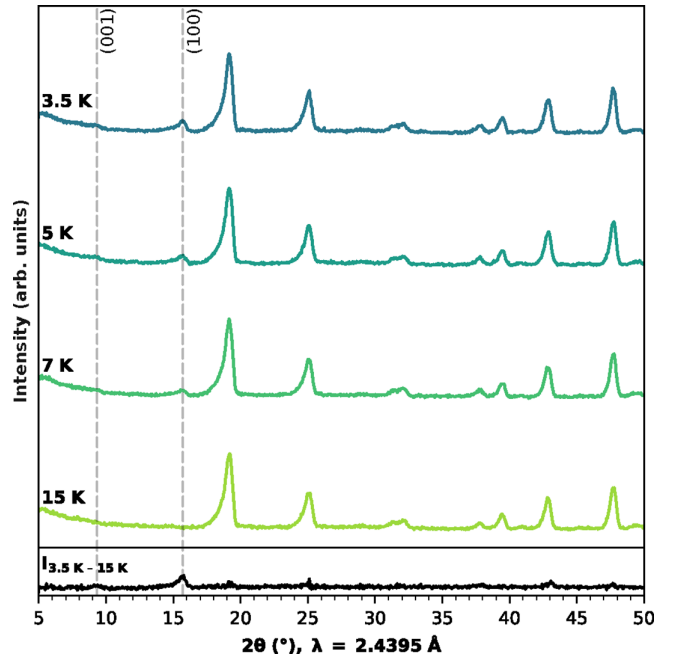

FIG. 5. Powder neutron diffraction scans for $Li_2Ni_2W_2O_9$ powder, from $T = 15$ K (light green) to $T = 3.5$ K (blue). The difference between the diffractograms for $T = 3.5$ and 15 K is plotted in black at the bottom of the figure.

nickel cations can be paired in such a way that the magnetic components of each cation in a pair are reversed, and their coordinates systems are opposite to one another. Such pairs are Ni(1)/Ni(5), Ni(2)/Ni(6), Ni(3)/Ni(7), and Ni(4)/Ni(8). This indicates that the magnetic structure contains a time reversal center as well as an inversion center; the combination of these two symmetry elements is required in linear magnetoelectric materials.

To get into more details, the magnetic structure of $Li_2Ni_2W_2O_9$ can be broken down into three different scales: chain, layer, and stack of layers. Inside a Ni-Ni chain, a parallel alignment of the magnetic moments is observed. Meanwhile, inside a Ni-W layer, the magnetic moments of two neighboring chains display weak parallel alignment along the b axis, and a comparatively stronger antiparallel alignment along the c axis. Finally, these layers are piled into stacks along the c axis; the resulting magnetic moments of two neighboring layers in a stack are antiparallel to one another along the b axis (Fig. 9).

III. DISCUSSION

The crystal structure of $Li_2Ni_2W_2O_9$ leads to both superexchange (Ni-O-Ni) and super-superexchange (Ni-O-O-Ni)

interactions in the material. As the magnetic structure is long-range ordered, three distinct isotropic exchange interactions need to be considered: an intrachain double interaction J_1 (2.93 Å), an interchain interaction J_2 (3.40 Å), and an interlayer interaction J_3 (6.05 Å) (Fig. 9).

Between two closest neighbors in a NiO_6 chain (J_1), two superexchange paths exist. These paths are characterized by a $\sim 90°$ Ni-O-Ni angle (Table IV), leading to ferromagnetic interactions in accordance to the Goodenough-Kanamori-Anderson rules [34–36]. Meanwhile, for interchain interaction J_2, the orientation of the magnetic moments of the nickel cations ($\mathbf{m}_b$ components parallel and $\mathbf{m}_c$ components antiparallel) suggest some competition between ferromagnetic and antiferromagnetic interactions. The former could be coming from the superexchange path of J_2, as the $112.01°$ Ni-O-Ni angle is closer to $90°$ than $180°$, probably below the ferromagnetic-to-antiferromagnetic critical angle described by Goodenough [34]; but again, this is mostly speculative, and an analysis based solely on geometry might miss some other important factors influencing the magnetic structure. The super-superexchange path of J_3 leads to antiferromag-

TABLE II. Results of the modified Curie-Weiss fits for the $1/\chi_m$ vs T curves.

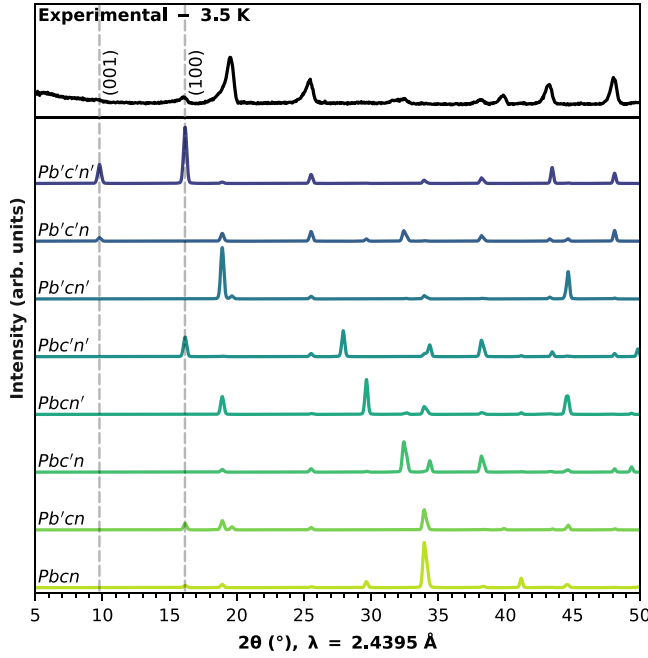|		θ_{CW} (K)	C (10^{-5} m^3 K mol^{-1})	μ_{eff} (μ_B)	Fitting range (K)
$H = 200$ Oe	ZFC	15.09(2)	1.7228(9)	3.32(8)	[50; 300]
	FC	8.8(1)	2.208(6)	3.8(2)	[50; 200]
$H = 1$ kOe	ZFC	13.68(3)	1.680(1)	3.28(8)	[50; 250]
	FC	12.85(4)	1.731(1)	3.33(8)	[50; 250]
$H = 10$ kOe	ZFC	13.99(3)	1.8303(4)	3.42(5)	[50; 300]
	FC	13.98(1)	1.8196(4)	3.41(5)	[50; 300]

FIG. 6. Experimental (black curve, top) and simulated (colored curves) diffraction patterns of $Li_2Ni_2W_2O_9$. The simulated curves were plotted with $M_y = 0.5\,\mu_B$ and $M_z = 1.5\,\mu_B$. Theoretical data for the 8 magnetic space groups were taken from the MAXMAGN software [7] of the Bilbao Crystallographic Server [8–10].

FIG. 7. Rietveld refinement for the neutron powder diffraction data of $Li_2Ni_2W_2O_9$ at $T = 15$ K in the $Pbcn$ nuclear space group (top) and at $T = 3.5$ K in the $Pb'c'n'$ Shubnikov space group (#60.425; middle). Bottom: Rietveld refinement against the difference curve between the neutron powder diffraction data of $Li_2Ni_2W_2O_9$ at $T = 3.5$ and 15 K.

netic interactions between the (Ni, W) layers without too much ambiguity; this can be explained quite well, again, by the Goodenough-Kanamori-Anderson rules, and by the 180° Ni-O-O-Ni dihedral angle.

In any case, the nature of these magnetic interactions explains the unusual behavior observed in the magnetization measurements: although the structure is antiferromagnetic overall, the Curie-Weiss temperature for $Li_2Ni_2W_2O_9$ is positive because of the intrachain and interchain ferromagnetic interactions. Moreover, looking at the topology of J_1, J_2, and J_3 [Figs. 9(b) and 9(c)], it is interesting to observe that the magnetic connectivity of the nickel cations leads to hexagonal magnetic loops; as there are no odd-sided loops, the magnetic structure is not geometrically frustrated. This observation matches well with the low values of the frustration index calculated earlier.
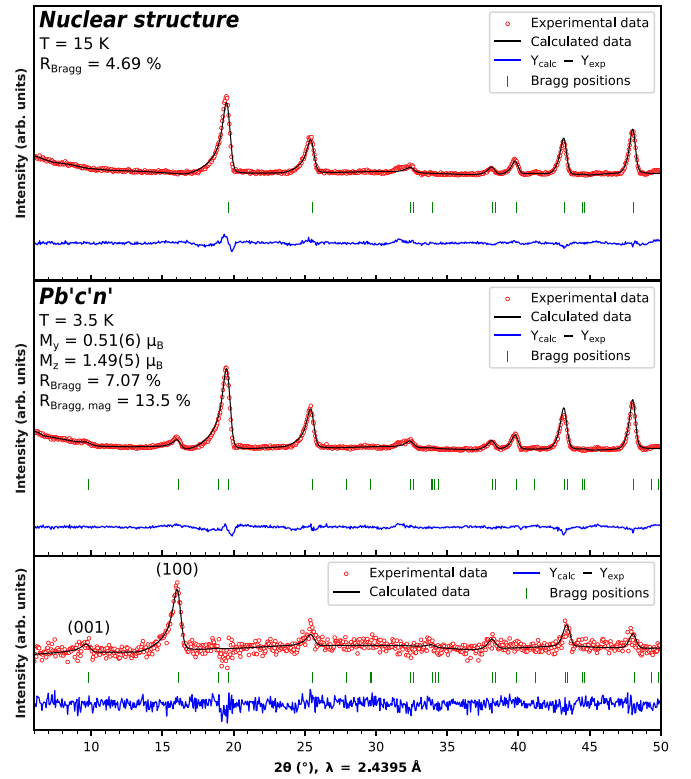
These considerations not only fit with the $Pb'c'n'$ space group, they also make it rather unlikely that the magnetic space group of $Li_2Ni_2W_2O_9$ is $Pbcn$. Looking at the theoretical magnetic structure associated with the $Pbcn$ Shubnikov space group (Fig. S10 in the Supplemental Material [30]), one can notice that the intrachain magnetic interactions would be mostly antiferromagnetic. Not only would this go against the Goodenough-Kanamori-Anderson rules, it would also go against the experimental results, namely, the high ferromagnetic interactions observed in the magnetic measurements. Considering said measurements, and considering that J_1, as

TABLE III. Magnetic structure of $Li_2Ni_2W_2O_9$ as deduced from the Rietveld refinement of the neutron diffraction pattern measured at 3.5 K.

Shubnikov magnetic space group: $Pb'c'n'$, $\mathbf{k} = (0, 0, 0)$, $R_{Bragg} = 7.07\%$, $R_{Bragg,\ magn} = 13.5\%$, $\chi^2 = 10.2$

| Cation	Coordinates	x/a	y/b	z/c	$M_y\ (\mu_B)$	$M_z\ (\mu_B)$
Ni(1)	x, y, z	0.6648(5)	0.512(11)	0.8136(18)	+0.51(6)	+1.49(5)
Ni(2)	$\bar{x} + \frac{1}{2}, \bar{y} + \frac{1}{2}, z + \frac{1}{2}$	0.8352(5)	0.988(11)	0.3136(18)	−0.51(6)	+1.49(5)
Ni(3)	$\bar{x}, y, \bar{z} + \frac{1}{2}$	0.3352(5)	0.512(11)	0.6864(18)	+0.51(6)	−1.49(5)
Ni(4)	$x + \frac{1}{2}, \bar{y} + \frac{1}{2}, \bar{z}$	0.1648(5)	0.988(11)	0.1864(18)	−0.51(6)	−1.49(5)
Ni(5)	$\bar{x}, \bar{y}, \bar{z}$	0.3352(5)	0.488(11)	0.1864(18)	−0.51(6)	−1.49(5)
Ni(6)	$x + \frac{1}{2}, y + \frac{1}{2}, \bar{z} + \frac{1}{2}$	0.1648(5)	0.012(11)	0.6864(18)	+0.51(6)	−1.49(5)
Ni(7)	$x, \bar{y}, z + \frac{1}{2}$	0.6648(5)	0.488(11)	0.3136(18)	−0.51(6)	+1.49(5)
Ni(8)	$\bar{x} + \frac{1}{2}, y + \frac{1}{2}, z$	0.8352(5)	0.012(11)	0.8136(18)	+0.51(6)	+1.49(5)
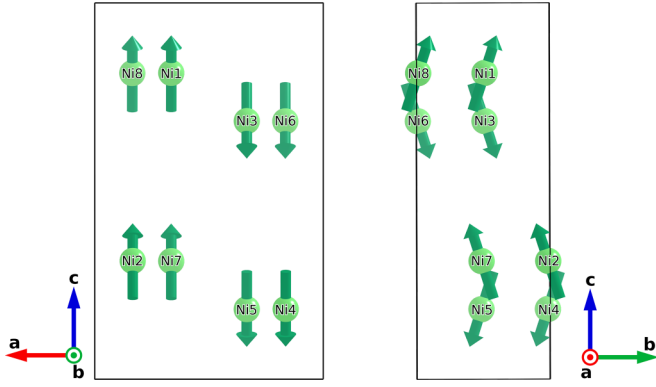
FIG. 8. Magnetic structure of $Li_2Ni_2W_2O_9$. Magnetic moments are represented by green arrows. For the sake of clarity, only nickel atoms are shown in the figure.

the shortest magnetic interaction path is also likely to be the strongest, it can be confidently ascertained that the intrachain interactions in $Li_2Ni_2W_2O_9$ must be ferromagnetic. Thus, the *Pbcn* magnetic space group is ruled out, and only *Pb'c'n'* remains.

In Fig. 10 is displayed a phase diagram showing the possible ground-state magnetic structures of $Li_2Ni_2W_2O_9$, depending on the values of the propagation vector **k** and of the exchange integrals J_1, J_2, and J_3.

This phase diagram was calculated by using the programs SIMBO and ENERMAG; El Khayati *et al.* [37] gave a full description of these programs, and the theory behind them can

be found in other works [38–41]. The magnetic ground state (or first-ordered state) is obtained, as a function of **k** and the exchange integrals J_{ij}, as the eigenvector corresponding to the lowest eigenvalue of the negative Fourier transform of the exchange integral matrix:

$$\xi_{ij}(\mathbf{k}) = -\sum_m J_{ij}(\mathbf{R}_m)\exp(-2\pi i\mathbf{k} \cdot \mathbf{R}_m), \quad (4)$$

where $J_{ij}(\mathbf{R}_m)$ is the isotropic exchange interaction between the spins of atoms i and j in unit cells separated by the lattice vector $\mathbf{R}_m$. As a convention, a negative value of the exchange interaction J_{ij} means that there is an antiparallel coupling between the spins $\mathbf{S}_i$ and $\mathbf{S}_j$, leading to the expression of the pair interaction energy shown in Eq. (5):

$$E_{ij} = -J_{ij}\mathbf{S}_i \cdot \mathbf{S}_j. \quad (5)$$

To build the phase diagram, we used a procedure which was applied to several magnetic structures in the past [33,42–47]. In a few words, the exchange integral matrixes $\boldsymbol{\xi}(\mathbf{k}, J_1, J_2, J_3)$ were calculated for values of J_1, J_2, J_3 ranging from -100 to 100, and for each set of values (J_1, J_2, J_3), the magnetic structure of lowest energy was selected. For all regions of the phase diagram, the lowest energy was obtained for $\mathbf{k} = (0, 0, 0)$; thus, only the spin sequence varies from one magnetic structure to the other.

The magnetic ground state of $Li_2Ni_2W_2O_9$ is split between two parts of the phase diagram. Although it is clear that $J_1 > 0$ and $J_3 < 0$, the value of J_2 is not the same depending on the component of the magnetic moments which is considered:
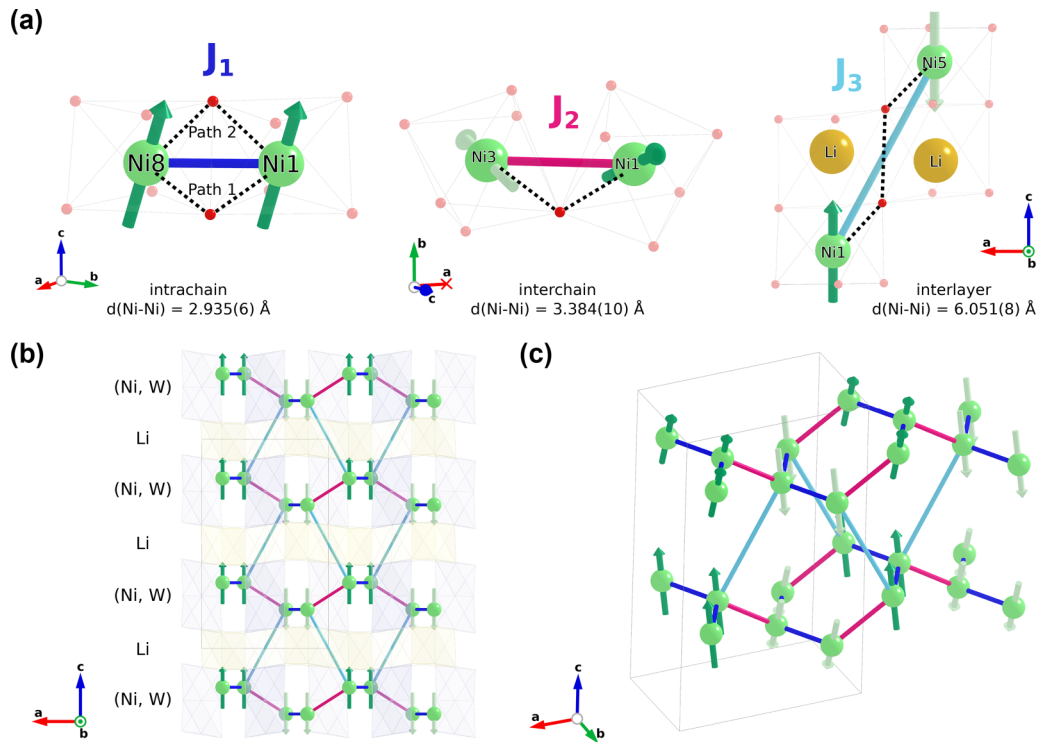

FIG. 9. Magnetic interaction paths in $Li_2Ni_2W_2O_9$. In (a), superexchange and super-superexchange paths are shown as black dotted lines. Nickel atoms are shown in green, lithium atoms in yellow, and oxygen atoms in red. In (b), WO_6 and LiO_6 octahedra are, respectively, shown in pale blue and in pale yellow. Magnetic moments with a positive M_z component are shown in dark green, while those with a negative M_z component are shown in light green.

TABLE IV. Geometric characteristics of the superexchange (Ni-O-Ni) and super-superexchange (Ni-O-O-Ni) paths for exchange interactions J_1, J_2, and J_3. Ni-O-O-Ni is the dihedral angle in degrees for the super-superexchange path.

Path	Distances (Å)				Angles (deg.)			
	d(Ni-Ni)	d(Ni-O)	d(O-O)	d(O-Ni)	Ni-O-Ni	Ni-O-O	O-O-Ni	Ni-O-O-Ni
J_1-Path 1-super	2.935(6)	1.982(7)	–	2.047(6)	93.51(17)	–	–	–
J_1-Path 2-super	2.935(6)	2.104(5)	–	2.118(7)	88.07(16)	–	–	–
J_2-super	3.384(10)	2.033(6)	–	2.033(6)	112.7(4)	–	–	–
J_3-super-super	6.051(8)	2.108(5)	3.19738(5)	2.108(5)	–	108.64(16)	108.64(16)	180.00

indeed, $J_2 > 0$ for $\mathbf{m}_b$, and $J_2 < 0$ for $\mathbf{m}_c$. This, again, highlights the dual nature of the J_2 interaction, both ferromagnetic and antiferromagnetic.

Another point to comment on relates to the magnetic space group of $Li_2Ni_2W_2O_9$, its nuclear structure, and potential magnetoelectric properties. It has been shown that the existence of such properties in a material is dependent upon the point symmetry of its magnetic structure [7–11]. The $m'm'm'$ point group allows for the magnetoelectric effect to manifest, as the diagonal components of the associated magnetoelectric tensor are nonzero [9,10]. This means that this effect could be present in $Li_2Ni_2W_2O_9$ because of its $Pb'c'n'$ magnetic space group. This is interesting because, as said earlier, the corundumlike structure of $Li_2Ni_2W_2O_9$ is very similar to that of 429 magnetic compounds [1], especially $Ni_4Nb_2O_9$, which crystallizes in the same orthorhombic nuclear space group [18]. However, ferrimagnetic ordering in $Ni_4Nb_2O_9$ occurs in the $Pb'cn'$ magnetic space group [19,24], corresponding to the magnetic point group $m'm'm$ (#8.4.27), which is not compatible with the linear magnetoelectric effect. Meanwhile, 429 compounds crystallizing in a trigonal space group $P\bar{3}c1$ ($Co_4Nb_2O_9$, $Co_4Ta_2O_9$, $Mn_4Nb_2O_9$, $Mn_4Ta_2O_9$, etc.) usually display linear magnetoelectric coupling [2,13,48,49]. Thus, $Li_2Ni_2W_2O_9$ might be the gateway to the exploration of

a magnetoelectric effect based on Ni^{2+} in a corundumlike orthorhombic structure. Moreover, as far as we can tell, substitution of the Ni^{2+} cations with other magnetic $3d$ transition metals (Co^{2+}, Fe^{2+}, etc.) has not yet been achieved in $Li_2Ni_2W_2O_9$; such an endeavor could potentially lead to other interesting magnetic compounds.

Compared with members of the 429 family, the magnetic transition temperature for $Li_2Ni_2W_2O_9$ ($T_N \approx 8\,K$) is much lower. $Fe_4Nb_2O_9$ displays two temperatures of transition, $T_{N1} \approx 90\,K$ and $T_{N2} \approx 80\,K$ [5,17]. In $Co_4Nb_2O_9$, the Néel point has been reported at $T_N = 27\,K$ [16,50]; meanwhile, in $Co_4Ta_2O_9$, various studies find $T_N \approx 20\,K$ [48,51,52]. Even $Ni_4Nb_2O_9$, a material with Ni^{2+} as the paramagnetic cation, displays a Curie temperature T_C equal to 76 K [19,20,24]. These major differences suggest that the magnetic interactions are weaker in $Li_2Ni_2W_2O_9$ than in 429 compounds. This could be due to a number of factors. First, the lower amount of magnetic cations per formula unit could introduce some sort of diamagnetic dilution effect. Such a phenomenon was reported by Tarakina $et\ al.$ [25] in $MgNi_3Nb_2O_9$. Another factor, related to the one described above, is the difference in crystal structure between $Li_2Ni_2W_2O_9$ and the $M_4A_2O_9$ compounds. Whereas $Ni_4Nb_2O_9$, for instance, displays two types of magnetic layers [the (Ni2, Nb) double layer and

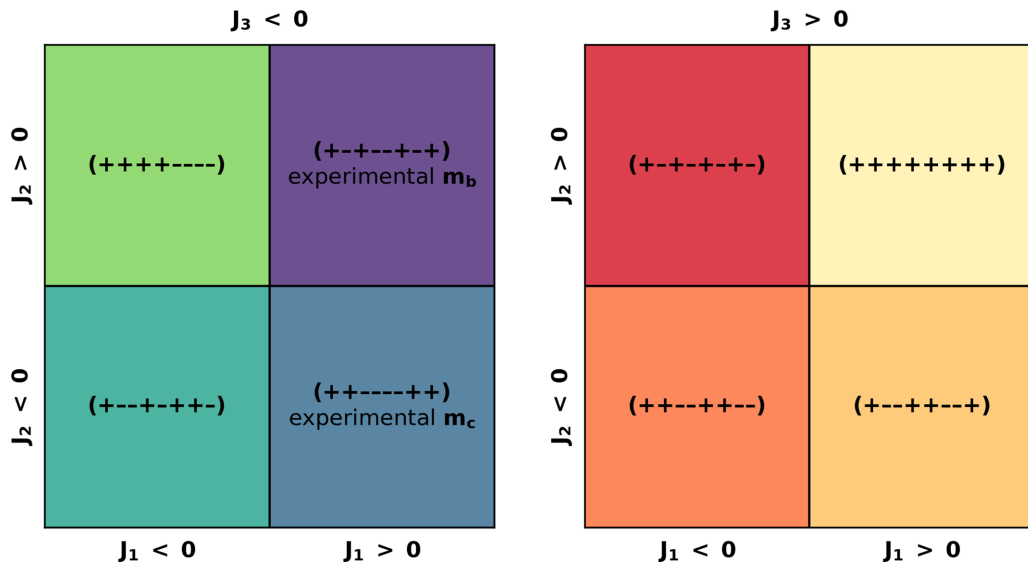FIG. 10. Phase diagram showing the possible magnetic ground states of $Li_2Ni_2W_2O_9$ below T_N as a function of the values of the exchange integrals J_1, J_2, and J_3. $\mathbf{k} = (0, 0, 0)$ in all ground-states. The ground-state magnetic structures observed experimentally from the neutron diffraction data shown in Fig. 3 are indicated in the purple and blue parts of the diagram.

the Ni1 single layer], paramagnetic (with unpaired electrons) Ni^{2+} cations in $Li_2Ni_2W_2O_9$ are only present in (Ni, W) double layers, separated by diamagnetic (without unpaired electrons) Li^+ interlayers (Fig. 1). As such, the distance along the c axis between two paramagnetic Ni^{2+} cations is much longer in $Li_2Ni_2W_2O_9$ $[d_{J3}(Ni - Ni) = 6.051(8) Å]$ than in $Ni_4Nb_2O_9$ $[d(Ni1 - Ni2) = 2.659(3) Å]$ [24]. This means that the magnetic interactions are likely much weaker between two successive paramagnetic layers in $Li_2Ni_2W_2O_9$ than in other 429 compounds. Finally, one may wonder whether or not replacing the Nb^{5+}/Ta^{5+} cations by W^{6+} cations has an impact on the magnetic properties, even though NbO_6, TaO_6, and WO_6 are all distorted by the same second-order Jahn-Teller effect [53,54].

It is also interesting to observe that, although it displays the same antiferromagnetic ordering as many of the 429 compounds [1,5,6,51], $Li_2Ni_2W_2O_9$ distinguishes itself by displaying a positive Curie-Weiss temperature $\theta_{CW} \approx 14$ K, whereas all 429 compounds show $\theta_{CW} < 0$. Even $Ni_4Nb_2O_9$ displays a strongly negative Curie-Weiss temperature ($\theta_{CW} = -233$ K), even though it is distinct from other 429 compounds for having a parallel alignment of the Ni^{2+} magnetic moments in its Ni1 single layer and of those in its (Ni2, Nb) double layer [19,24]. This again shows how the introduction of the Li^+ interlayer changes the magnetic interactions in $Li_2Ni_2W_2O_9$. Compared with $Ni_4Nb_2O_9$, for which the Ni1-Ni2 antiferromagnetic interactions are the strongest in the material, the intrachain ferromagnetic Ni-Ni interactions dominate in $Li_2Ni_2W_2O_9$. Meanwhile, the $P\bar{3}c1$ structure of other 429 compounds usually leads to strong antiferromagnetic intralayer interactions and weak ferromagnetic interlayer interactions [15,17,51,55]. As such, the crystal structure of $Li_2Ni_2W_2O_9$ introduces favored ferromagnetic interactions in the general antiferromagnetic order usually found in 429 compounds.

IV. CONCLUSIONS

Herein, we gave a first overview of the magnetic properties of layered $Li_2Ni_2W_2O_9$. The material becomes antiferromagnetically ordered below $T_N \approx 8$ K, but only for $|H| < 8$ kOe. Moreover, although magnetic measurements clearly indicate an antiferromagnetic ordering, subsequent modified Curie-Weiss fits point to the presence of strong ferromagnetic interactions, with low frustration. This apparent contradiction was explained by solving the magnetic structure of $Li_2Ni_2W_2O_9$, through low-temperature neutron powder diffraction ($T < T_N$). Although the magnetic moments are arranged in an antiferromagnetic configuration overall, the magnetic lattice is organized in three different subscales: in a (Ni,W) layer, ferromagnetic NiO_6 chains are coupled antiferromagnetically along c and ferromagnetically along b. Meanwhile, the coupling between two subsequent (Ni,W) layer is antiferromagnetic. This peculiar magnetic structure fits in the $Pb'c'n'$ magnetic space group, which by symmetry allows the linear magnetoelectric effect. Further experiments are required to fully explore all the magnetic properties of $Li_2Ni_2W_2O_9$, especially regarding possible metamagnetism and magnetoelectric effects.

ACKNOWLEDGMENTS

[1] E. F. Bertaut, L. Corliss, F. Forrat, R. Aleonard, and R. Pauthenet, Etude de niobates et tantalates de metaux de transition bivalents, J. Phys. Chem. Solids **21**, 234 (1961).

[2] E. Fischer, G. Gorodetsky, and R. M. Hornreich, A new family of magnetoelectric materials: $A_2M_4O_9$ ($A =$ Ta, Nb; $M =$ Mn, Co), Solid State Commun. **10**, 1127 (1972).

[3] B. Schwarz, D. Kraft, R. Theissmann, and H. Ehrenberg, Magnetic properties of the $(Co_xMn_{1-x})_4Nb_2O_9$ solid solution series, J. Magn. Magn. Mater. **322**, L1 (2010).

[4] Y. Fang, W. P. Zhou, S. M. Yan, R. Bai, Z. H. Qian, Q. Y. Xu, D. H. Wang, and Y. W. Du, Magnetic-field-induced dielectric anomaly and electric polarization in $Mn_4Nb_2O_9$, J. Appl. Phys. **117**, 17B712 (2015).

[5] A. Maignan and C. Martin, $Fe_4Nb_2O_9$: A magnetoelectric antiferromagnet, Phys. Rev. B **97**, 161106(R) (2018).

[6] Y. Cao, K. Xu, Y. Yang, W. Yang, Y. Zhang, Y. Kang, X. He, A. Zheng, M. Liu, S. Wei *et al.*, High-quality single crystal growth and magnetic property of $Mn_4Ta_2O_9$, J. Cryst. Growth **492**, 35 (2018).

[7] P. Curie, Sur la symétrie dans les phénomènes physiques, symétrie d'un champ électrique et d'un champ magnétique, J. Phys. Theor. Appl. **3**, 393 (1894).

[8] R. R. Birss, Macroscopic symmetry in space-time, Rep. Prog. Phys. **26**, 307 (1963).

[9] T. H. O'Dell, *The Electrodynamics of Magneto-Electric Media* (North-Holland Publishing Company, Amsterdam, and American Elsevier Publishing Company Inc., New York, 1970).

[10] J.-P. Rivera, On definitions, units, measurements, tensor forms of the linear magnetoelectric effect and on a new dynamic method applied to Cr-Cl boracite, Ferroelectrics **161**, 165 (1994).

[11] H. Schmid, Some symmetry aspects of ferroics and single phase multiferroics, J. Phys. Condens. Matter **20**, 434201 (2008).

[12] L. Pauling and S. B. Hendricks, The crystal structures of hematite and corundum, J. Am. Chem. Soc. **47**, 781 (1925).

[13] N. D. Khanh, N. Abe, H. Sagayama, A. Nakao, T. Hanashima, R. Kiyanagi, Y. Tokunaga, and T. Arima, Magnetoelectric coupling in the honeycomb antiferromagnet $Co_4Nb_2O_9$, Phys. Rev. B **93**, 075117 (2016).

[14] N. D. Khanh, N. Abe, S. Kimura, Y. Tokunaga, and T. Arima, Manipulation of electric polarization with rotating magnetic field in a honeycomb antiferromagnet $Co_4Nb_2O_9$, Phys. Rev. B **96**, 094434 (2017).

[15] G. Deng, Y. Cao, W. Ren, S. Cao, A. J. Studer, N. Gauthier, M. Kenzelmann, G. Davidson, K. C. Rule, J. S. Gardner *et al.*, Spin dynamics and magnetoelectric coupling mechanism of $Co_4Nb_2O_9$, Phys. Rev. B **97**, 085154 (2018).

[16] L. Ding, M. Lee, T. Hong, Z. Dun, R. Sinclair, S. Chi, H. K. Agrawal, E. S. Choi, B. C. Chakoumakos, H. Zhou *et al.*, Noncollinear magnetic structure and magnetoelectric coupling in buckled honeycomb $Co_4Nb_2O_9$: A single-crystal neutron diffraction study, Phys. Rev. B **102**, 174443 (2020).

[17] R. Jana, D. Sheptyakov, X. Ma, J. A. Alonso, M. Pi, A. Muñoz, Z. Liu, L. Zhao, N. Su, S. Jin *et al.*, Low-temperature crystal and magnetic structures of the magnetoelectric material $Fe_4Nb_2O_9$, Phys. Rev. B **100**, 094109 (2019).

[18] R. Wichmann and Hk. Müller-Buschbaum, Eine neue Kristallstruktur des Nickel-Oxoniobats: II-$Ni_4Nb_2O_9$, Z. Für Anorg. Allg. Chem. **539**, 203 (1986).

[19] H. Ehrenberg, G. Wltschek, H. Weitzel, F. Trouw, J. H. Buettner, T. Kroener, and H. Fuess, Ferrimagnetism in $Ni_4Nb_2O_9$, Phys. Rev. B **52**, 9595 (1995).

[20] S. Thota, M. S. Seehra, M. R. Chowdhury, H. Singh, S. Ghosh, S. K. Jena, P. Pramanik, T. Sarkar, R. S. Rawat, R. Medwal *et al.*, Unraveling the nature of ferrimagnetism and associated exchange interactions in distorted honeycomb $Ni_4Nb_2O_9$, Phys. Rev. B **106**, 134418 (2022).

[21] J. P. Bolletta, F. Fauth, C. Martin, and A. Maignan, Magnetization reversal tuning in honeycomb ferrimagnet $Ni_4Nb_2O_9$, J. Appl. Phys. **132**, 153901 (2022).

[22] J. N. Jiongo-Dongmo, J. P. Bolletta, A. Maignan, F. Damay, and C. Martin, The $Ni_{4-x}Co_xNb_2O_9$ phase diagram: From magnetization reversal to linear magnetoelectricity, J. Mater. Chem. C **11**, 5092 (2023).

[23] B. Meng, X. T. Ji, X. H. Chen, Q. S. Fu, C. L. Li, C. Chakrabarti, Y. Qiu, and S. L. Yuan, Negative magnetization effect in distorted honeycomb $Ni_4Nb_2O_9$ ceramics, J. Low Temp. Phys. **207**, 115 (2022).

[24] E. Tailleur, C. Martin, F. Damay, F. Fauth, and A. Maignan, Lack of linear magnetoelectric effect in ferrimagnetic distorted honeycomb $Ni_4Nb_2O_9$, J. Appl. Phys. **127**, 063902 (2020).

[25] N. V. Tarakina, E. A. Nikulina, J. Hadermann, D. G. Kellerman, A. P. Tyutyunnik, I. F. Berger, V. G. Zubkov, and G. Van Tendeloo, Crystal structure and magnetic properties of complex oxides $Mg_{4-x}Ni_xNb_2O_9$, $0 \leqslant x \leqslant 4$, J. Solid State Chem. **180**, 3180 (2007).

[26] S. Redor, L. Godeffroy, G. Rousse, A. M. Abakumov, B. Li, F. Kanoufi, and J.-M. Tarascon, Electrochromic corundum-like compound based on the reversible (De)insertion of lithium: $Li_2Ni_2W_2O_9$, J. Am. Chem. Soc. **145**, 12823 (2023).

[27] M. Avdeev and J. R. Hester, ECHIDNA: A decade of high-resolution neutron powder diffraction at OPAL, J. Appl. Cryst. **51**, 1597 (2018).

[28] H. M. Rietveld, A profile refinement method for nuclear and magnetic structures, J. Appl. Cryst. **2**, 65 (1969).

[29] J. Rodríguez-Carvajal, Recent advances in magnetic structure determination by neutron powder diffraction, Phys. B Condens. Matter **192**, 55 (1993).

[30] See Supplemental Material at http://link.aps.org/supplemental/10.1103/PhysRevB.109.054105 for the detailed results of the Rietveld refinements performed on the laboratory XRD and neutron powder diffraction data for $Li_2Ni_2W_2O_9$ samples. Simulations of neutron powder diffraction patterns for different models of the magnetic structure, and the .mcif file for the final magnetic structure of $Li_2Ni_2W_2O_9$ are also included.

[31] E. Stryjewski and N. Giordano, Metamagnetism, Adv. Phys. **26**, 487 (1977).

[32] J. I. Hoppeé, Effective magnetic moment, J. Chem. Educ. **49**, 505 (1972).

[33] M. Reynaud, J. Rodríguez-Carvajal, J.-N. Chotard, J.-M. Tarascon, and G. Rousse, Magnetic structure and properties of orthorhombic $Li_2Ni(SO_4)_2$: A possible magnetoelectric material, Phys. Rev. B **89**, 104419 (2014).

[34] J. B. Goodenough, *Magnetism and the Chemical Bond* (Interscience Publishers, New York, 1963).

[35] J. B. Goodenough, An interpretation of the magnetic properties of the perovskite-type mixed crystals $La_{1-x}Sr_xCoO_{3-\lambda}$, J. Phys. Chem. Solids **6**, 287 (1958).

[36] J. Kanamori, Superexchange interaction and symmetry properties of electron orbitals, J. Phys. Chem. Solids **10**, 87 (1959).

[37] N. El Khayati, R. Cherkaoui El Moursli, J. Rodríguez-Carvajal, G. André, N. Blanchard, F. Bourée, G. Collin, and T. Roisnel, Crystal and magnetic structures of the oxyphosphates $MFePO_5$ (M = Fe, Co, Ni, Cu). Analysis of the magnetic ground state in terms of superexchange interactions, Eur. Phys. J. B **22**, 429 (2001).

[38] A. Yoshimori, A new type of antiferromagnetic structure in the rutile type crystal, J. Phys. Soc. Jpn. **14**, 807 (1959).

[39] J. Villain, La structure des substances magnetiques, J. Phys. Chem. Solids **11**, 303 (1959).

[40] D. H. Lyons and T. A. Kaplan, Method for determining ground-state spin configurations, Phys. Rev. **120**, 1580 (1960).

[41] M. J. Freiser, Thermal variation of the pitch of helical spin configurations, Phys. Rev. **123**, 2003 (1961).

[42] M. Reynaud, G. Rousse, J.-N. Chotard, J. Rodríguez-Carvajal, and J.-M. Tarascon, Marinite $Li_2M(SO_4)_2$ (M = Co, Fe, Mn) and $Li_1Fe(SO_4)_2$: Model compounds for super-super-exchange magnetic interactions, Inorg. Chem. **52**, 10456 (2013).

[43] G. Rousse, J. Rodríguez-Carvajal, C. Wurm, and C. Masquelier, Magnetic structural studies of the two polymorphs of $Li_3Fe_2(PO_4)_3$: Analysis of the magnetic ground state from super-super exchange interactions, Chem. Mater. **13**, 4527 (2001).

[44] G. Rousse, J. Rodriguez-Carvajal, S. Patoux, and C. Masquelier, Magnetic structures of the triphylite $LiFePO_4$ and of its delithiated form $FePO_4$, Chem. Mater. **15**, 4082 (2003).

[45] B. C. Melot, G. Rousse, J.-N. Chotard, M. Ati, J. Rodríguez-Carvajal, M. C. Kemei, and J.-M. Tarascon, Magnetic structure and properties of the Li-ion battery materials $FeSO_4F$ and $LiFeSO_4F$, Chem. Mater. **23**, 2922 (2011).

[46] B. C. Melot, G. Rousse, J.-N. Chotard, M. C. Kemei, J. Rodríguez-Carvajal, and J.-M. Tarascon, Magnetic structure and properties of $NaFeSO_4F$ and $NaCoSO_4F$, Phys. Rev. B **85**, 094415 (2012).

[47] S. Ghara, F. Fauth, E. Suard, J. Rodriquez-Carvajal, and A. Sundaresan, Synthesis, structure, and physical properties of the polar magnet $DyCrWO_6$, Inorg. Chem. **57**, 12827 (2018).

[48] S. Chaudhary, P. Srivastava, S. D. Kaushik, V. Siruguri, and S. Patnaik, Nature of magnetoelectric coupling in corundum antiferromagnet $Co_4Ta_2O_9$, J. Magn. Magn. Mater. **475**, 508 (2019).

[49] S. Chaudhary, V. Nagpal, and S. Patnaik, Magnetoelectric response in honeycomb antiferromagnet Fe_4NbTaO_9, J. Magn. Magn. Mater. **515**, 167305 (2020).

[50] Y. P. Lu, C. X. Ji, Y. L. Sun, Y. Fang, L. Zhang, Z. D. Han, B. Qian, X. F. Jiang, and W. P. Zhou, Magnetic, dielectric and magnetoelectric properties of polycrystalline $Nb_2Co_4O_9$, J. Alloys Compd. **679**, 213 (2016).

[51] N. Lee, D. G. Oh, S. Choi, J. Y. Moon, J. H. Kim, H. J. Shin, K. Son, J. Nuss, V. Kiryukhin, and Y. J. Choi, Highly nonlinear magnetoelectric effect in buckled-honeycomb antiferromagnetic $Co_4Ta_2O_9$, Sci. Rep. **10**, 12362 (2020).

[52] S. Choi, D. G. Oh, M. J. Gutmann, S. Pan, G. Kim, K. Son, J. Kim, N. Lee, S.-W. Cheong, Y. J. Choi *et al.*, Noncollinear antiferromagnetic order in the buckled honeycomb lattice of magnetoelectric $Co_4Ta_2O_9$ determined by single-crystal neutron diffraction, Phys. Rev. B **102**, 214404 (2020).

[53] M. Kunz and I. D. Brown, Out-of-center distortions around octahedrally coordinated d^0 transition metals, J. Solid State Chem. **115**, 395 (1995).

[54] S. K. Kang, H. Tang, and T. A. Albright, Structures for d^0 ML_6 and ML_5 complexes, J. Am. Chem. Soc. **115**, 1971 (1993).

[55] G. Deng, G. Zhao, S. Zhu, Z. Feng, W. Ren, S. Cao, A. Studer, and G. J. McIntyre, Spin dynamics, critical scattering and magnetoelectric coupling mechanism of $Mn_4Nb_2O_9$, New J. Phys. **24**, 083007 (2022).